HAL
open science

Refined finite element modelling for the vibration analysis of large rotating machines

Didier Combescure, Arnaud Lazarus

To cite this version:

Didier Combescure, Arnaud Lazarus. Refined finite element modelling for the vibration analysis of large rotating machines. Journal of Sound and Vibration, 2008, 318, 10.1016/j.jsv.2008.04.025 . hal-01452022

HAL Id: hal-01452022

https://hal.science/hal-01452022v1

Submitted on 25 Nov 2017

HAL is a multi-disciplinary open access archive for the deposit and dissemination of scientific research documents, whether they are published or not. The documents may come from teaching and research institutions in France or abroad, or from public or private research centers.

L'archive ouverte pluridisciplinaire **HAL**, est destinée au dépôt et à la diffusion de documents scientifiques de niveau recherche, publiés ou non, émanant des établissements d'enseignement et de recherche français ou étrangers, des laboratoires publics ou privés.

Refined finite element modelling for the vibration analysis of large rotating machines: Application to the gas turbine modular helium reactor power conversion unit

D. Combescure[a], A. Lazarus[a,b,*]

[a]*Dynamic Analysis Laboratory, CEA-DEN/DM2S/SEMT/DYN, CEA Saclay, France*
[b]*Laboratoire de Mécanique des Solides, Ecole Polytechnique, Palaiseau, France*

This paper is aimed at presenting refined finite element modelling used for dynamic analysis of large rotating machines. The first part shows an equivalence between several levels of modelling: firstly, models made of beam elements and rigid disc with gyroscopic coupling representing the position of the rotating shaft in an inertial frame; secondly full three-dimensional (3D) or 3D shell models of the rotor and the blades represented in the rotating frame and finally two-dimensional (2D) Fourier model for both rotor and stator. Simple cases are studied to better understand the results given by analysis performed using a rotating frame and the equivalence with the standard calculations with beam elements. Complete analysis of rotating machines can be performed with models in the frames best adapted for each part of the structure. The effects of several defects are analysed and compared with this approach. In the last part of the paper, the modelling approach is applied to the analysis of the large rotating shaft part of the power conversion unit of the GT-MHR nuclear reactor.

1. Introduction

Rotordynamics has a major importance for the development of new electricity production units. Safety and service life of turbo-alternator units and pumps are directly linked to a high-quality control of their vibratory behaviour. This is emphasized for the gas turbine modular helium reactor named as the GT-MHR reactor, which includes a large helium turbine directly in the first cycle of the high-temperature gas-cooled reactor (Fig. 1 [1–4]). Such large rotating machines require advanced modelling for design and predictive maintenance. Due to the severe environment, which limits the access to the turbine, refined dynamic analyses are necessary to anticipate potential vibration problems under normal and accidental loading. In particular, predictive modelling can help mass balancing and improving turbine maintenance.

*Corresponding author at: Dynamic Analysis Laboratory, CEA-DEN/DM2S/SEMT/DYN, CEA Saclay, France. Tel.: +33 1 69 08 87 53.
E-mail addresses: didier.combescure@cea.fr, arnaud.lazarus@cea.fr (A. Lazarus).

Nomenclature

$\mathbf{C}$	damping matrix
E	Young's modulus
f, f_0	whirl frequency (damped free oscillations) and natural frequency (undamped) (Hz)
$\mathbf{F}(t)$	vector of external forces
$\mathbf{G}$	gyroscopic coupling matrix
$\mathbf{G}_c$	Coriolis coupling matrix
$\mathbf{H}$	asymmetrical stiffness matrix (for internal viscous damping)
I, J	respectively, the inertia around the Ox or Oy axis and the Oz axis
$\mathbf{K}$	stiffness matrix
$\mathbf{K}_c$	spin softening
$\mathbf{K}_\sigma$	geometrical stiffness
$\mathbf{M}$	mass matrix
n_θ	Fourier mode number
R, R'	respectively, the inertial and rotating frame
u_x,u_y,u_z	displacement in the Ox, Oy and Oz directions
$\mathbf{U}$, $\mathbf{U}'$	respectively, the displacement vectors in the inertial and the rotating frame
θ_x,θ_y,θ_z	rotation around the Ox, Oy and Oz axis
μ	material viscosity (N s/m). In this paper, the viscous forces are proportional to the velocity. The damping matrix is proportional to the stiffness matrix.
ρ	material mass density
ϕ_x,ϕ_y,ϕ_z	rotation around the Ox, Oy and Oz axis
ω, ω_0	whirl angular frequency and natural angular frequency (rad/s)
Ω	rotating velocity

Dynamic studies of rotating machines are generally performed using, on the one hand, beam element models representing the position of the rotating shaft in an inertial frame and, on the other hand, three-dimensional (3D) or two-dimensional (2D) Fourier rotor models represented in the rotating frame.

The first representation is generally used for stability analysis and prediction of the global dynamic response under unbalanced loads taking into account the gyroscopic effects [5–7]. In some cases (cracked rotor for example), the mass or/and stiffness matrices used in the analysis become time dependent and the analysis requires much more complex tools [8–10].

The calculations in the rotating frame usually focus on particular components such as blades in turbomachines. The two main effects taken into account by the model are the stiffening due to the geometrical stiffness under the centrifugal forces and the spin softening caused by the follower nature of the centrifugal forces [6,7,11]. Usually, little stability analysis and rotor vibration prediction is performed with refined modelling specially in case of interactions between rotor and stator which are very important at critical speeds [11–14].

This paper is aimed at presenting an equivalence between these two levels of modelling in order to be able to perform complete analyses with models in the most adapted frames for each part of the structure: a rotor model in the rotating frame and the supports in the inertial frame. In the last section, this advanced modelling approach is applied to the analysis of the large rotating shaft of the GT-MHR reactor.

2. Classical beam type model

In order to highlight the main assumptions of the classical beam type model used classically in rotordynamics [5,6], this part briefly presents a beam model with shear deformation, gyroscopic effect and internal (or corotative) damping and its application to a rotating machine made of a disc fixed on a flexible rotor supported by two bearings.

2.1. Gyroscopic and damping matrices

Rotating machines specially with rotating speed comparable to the natural pulsations at rest and large rotational inertia are characterized by the gyroscopic forces. It is well known that these forces induce a coupling between the transverse velocities of the shaft. The modelling of a rotating machine requires an asymmetric pseudo-damping matrix named gyroscopic matrix [5–7]. The particular form of the matrix makes complex eigenmodes appear, forward modes having increasing frequencies and backward modes

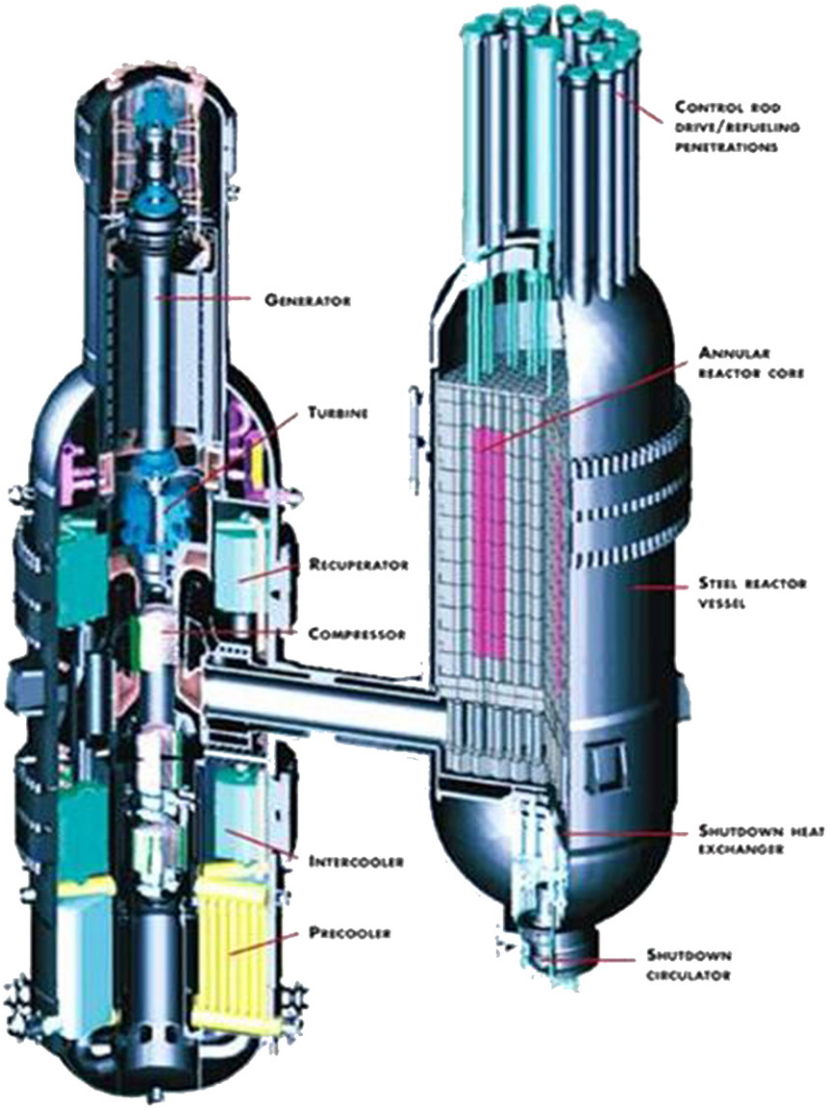

Fig. 1. Sketch of the GTMHR nuclear reactor (nuclear core on the right and power conversion unit on the left).

having decreasing frequencies. An example of a gyroscopic matrix is given for a disc (as moment-rotational velocity law):

$$\begin{Bmatrix} M_x \\ M_y \\ M_z \end{Bmatrix} = \mathbf{G} \cdot \begin{Bmatrix} \dot{\theta}_x \\ \dot{\theta}_y \\ \dot{\theta}_z \end{Bmatrix} = \Omega \rho J \begin{bmatrix} 0 & 1 & 0 \\ -1 & 0 & 0 \\ 0 & 0 & 0 \end{bmatrix} \cdot \begin{Bmatrix} \dot{\theta}_x \\ \dot{\theta}_y \\ \dot{\theta}_z \end{Bmatrix} \tag{1}$$

Oz is defined as the beam axis and ρJ the torsional inertia of the disc.

For beam elements, the gyroscopic matrix is computed by integration on the length of this elementary matrix assuming the torsional inertia constant on the length.

The degrees of freedom of the beam are not completely attached to the material frame but only to the centroid of the beam section. The mass and the stiffness matrices (respectively, **M** and **K**) used for the calculations are identical to the machine without rotation. These assumptions are realistic only in case of an isotropic beam section (uncracked rotor). Also in this case, precise modelling of damping of the rotating part

(internal damping) requires the use not only of a damping matrix but also of an asymmetrical stiffness matrix since the damping law of the rotor in the rotating frame is known and the change of frames (from the rotating frame R' where the damping matrix is defined to the inertial frame R where the calculation is performed) leads to a combination of velocities [5–7]. The damping matrix **C** and the asymmetrical pseudo-stiffness matrix **H** for a rotating beam section made of viscoelastic material can be determined by integration of the two moment-curvature laws:

$$\begin{Bmatrix} M_x \\ M_y \\ M_x \end{Bmatrix} = \begin{bmatrix} \mu I & 0 & 0 \\ 0 & \mu I & 0 \\ 0 & 0 & 0 \end{bmatrix} \cdot \begin{Bmatrix} \dot{\phi}_x \\ \dot{\phi}_y \\ \dot{\phi}_z \end{Bmatrix} \tag{2}$$

$$\begin{Bmatrix} M_x \\ M_y \\ M_x \end{Bmatrix} = \begin{bmatrix} 0 & \mu I\Omega & 0 \\ -\mu I\Omega & 0 & 0 \\ 0 & 0 & 0 \end{bmatrix} \cdot \begin{Bmatrix} \phi_x \\ \phi_y \\ \phi_x \end{Bmatrix} \tag{3}$$

Finally, the equilibrium equation of a rotating machine represented in the inertial frame can be written as follows:

$$\mathbf{M}\ddot{\mathbf{U}} + (\mathbf{G}(\Omega) + \mathbf{C}) \cdot \dot{\mathbf{U}} + (\mathbf{K} + \mathbf{H}(\Omega)) \cdot \mathbf{U} = \mathbf{F}(t) \tag{4}$$

2.2. First analysis of a rotating disc on a flexible shaft

A rotating disc fixed on a flexible shaft simply supported at each extremity has been studied in order to illustrate the main aspects of the analysis of rotating machines. Gyroscopic coupling and internal damping are included in the analysis.

The shaft described in Ref. [5] has a length $L_s = 0.40$ m and a radius $R_s = 0.01$ m. A disc, with a radius $R_d = 0.15$ m and a thickness $h_d = 0.005$ m, is fixed at one-third of the shaft length (Fig. 10a where the rotor is represented using 3D finite elements).

The evolution of complex frequencies is given in Fig. 2 (synchronous whirl is plotted to locate the critical speed). Complex eigenmodes are calculated after a preliminary projection of the equilibrium equation onto real eigenmodes at rest (Rayleigh–Ritz condensation). The gyroscopic coupling separates forward and backward eigenmodes. The critical speeds are defined as the rotating speed Ω which is equal to the natural frequency of one of the direct eigenmodes (both backward and forward eigenmodes for a non-isotropic rotor [5,6]). The first critical speed is about 700 rad/s which is slightly higher than the first natural angular frequency at rest (628 rad/s). Above the critical speed, damping of the forward mode becomes negative. Transient dynamic calculations have been performed for two rotation speeds (300 and 1200 rad/s) for an unbalance load at one-third of the shaft corresponding to an initial angular tilt of the disc (represented by a rotating concentrated couple). The trajectories of the disc centre are plotted in Fig. 3. It clearly shows that the forward mode of a supercritical machine is unstable due to the internal damping. The analysis of the response shows the unstable oscillations have the frequency of the forward mode and not the rotating frequency. It is well known that this risk of instability occurring in a supercritical rotor can be reduced using fixed damping [6,7].

Such a type of model remains linear under the assumptions of an isotropic shaft in stiffness but also in mass. If these assumptions are not verified (cracked rotor for example), the matrices used in the analysis become time dependent and the analysis requires much more complex tools (time-history analysis, parametric–dynamic equations, etc. [8–10]). An alternative is to perform the analysis with the rotor represented in the rotating frame and the stator in the inertial frame. The following sections illustrate this type of analysis.

3. Equations in the rotating frame

Modelling of flexible rotating machine requires more detailed kinematics than those of beam elements. This can be achieved using a rotating frame and 3D or 2D Fourier finite elements [11–13]. Let us describe such an

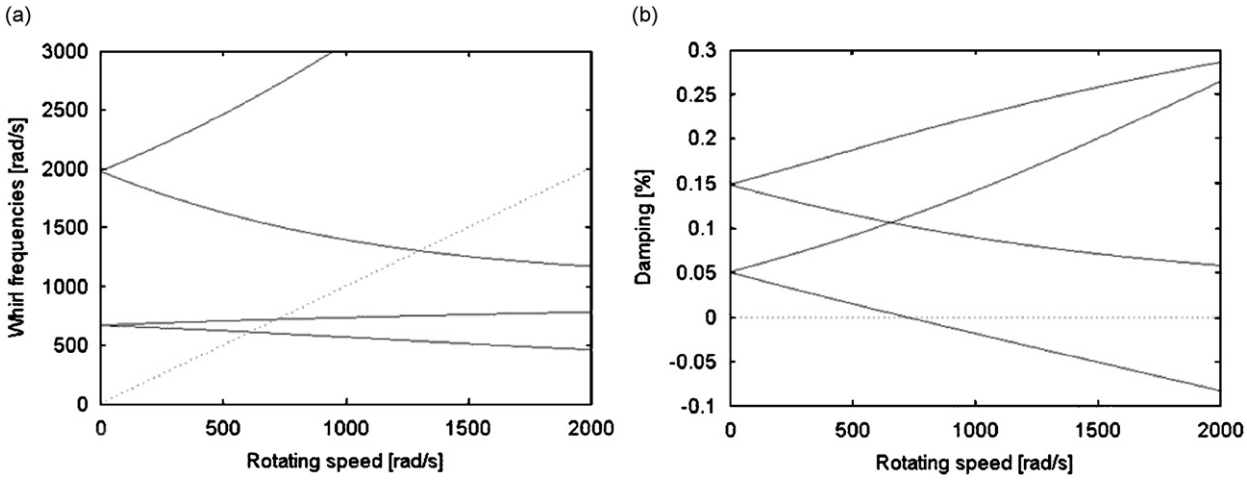

Fig. 2. Evolution of the complex frequencies of the shaft: (a) Whirl frequencies in full line. Synchronous whirl in dashed line. (b) Reduced damping values: imaginary part divided by the real part of the complex frequency (dynamic instability when negative).

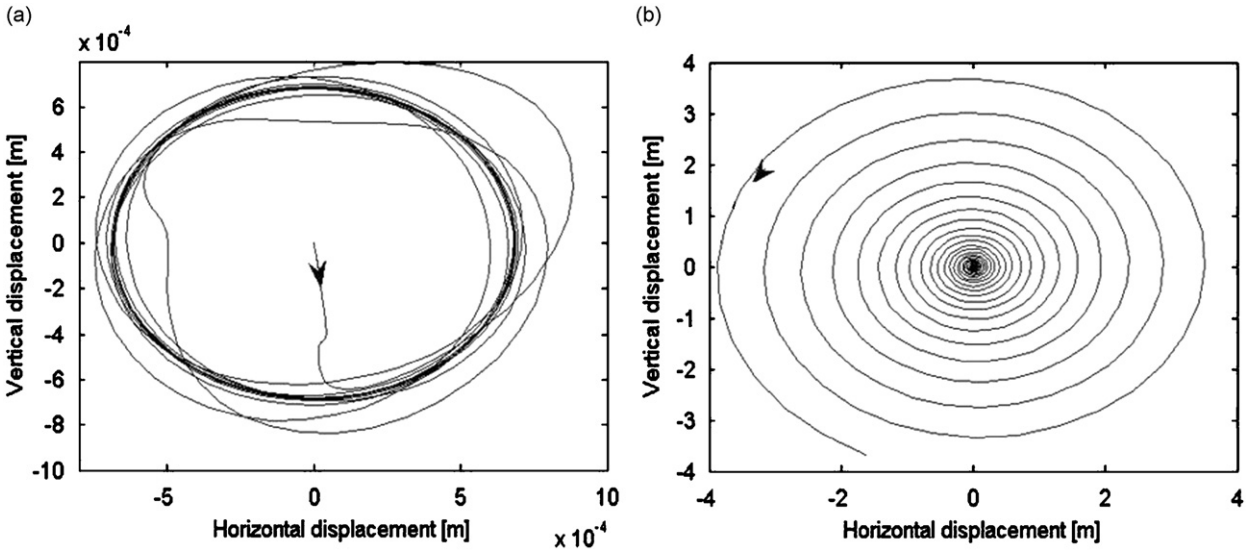

Fig. 3. Shaft trajectory for a transient unbalance load: (a) Undercritical regime $\Omega = 300\,\text{rad/s}$. (b) Supercritical regime $\Omega = 1200\,\text{rad/s}$.

approach, firstly, for a full 3D model and, secondly, for a 2D Fourier model. Examples of 3D and 2D models are given, respectively, in Sections 4 and 5.

3.1. 3D model

Let us recall the equations of motion in a rotating frame R' highlighting the main effects to be taken into account. The rotating speed Ω is assumed to be constant. The equilibrium equation has to take two aspects into account. Firstly, the Coriolis forces proportional to the velocities are represented by an asymmetrical pseudo-damping matrix. Secondly, the centrifugal forces apply to the deformed configuration. It means that these forces may change in amplitude or direction (Fig. 4). This requires the use of negative centrifugal stiffness (often named spin softening) and the geometrical stiffness.

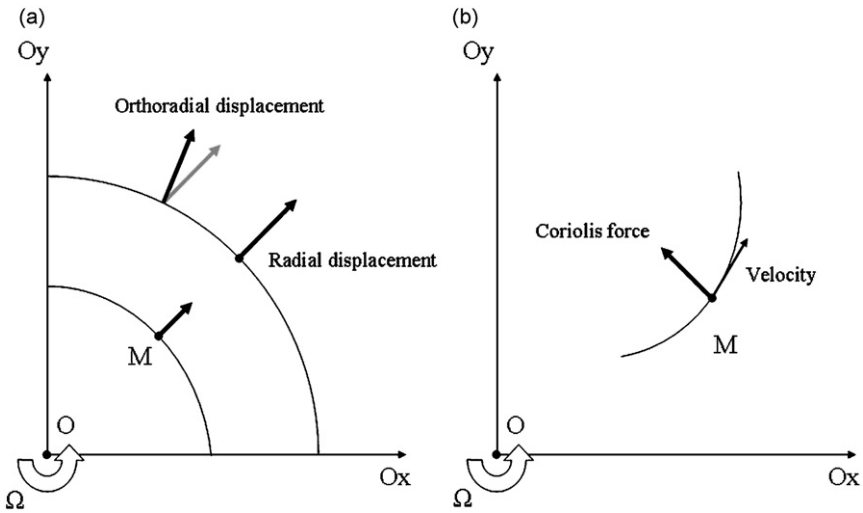

Fig. 4. Effect of motion in the rotating frame: (a) on the centrifugal force (b) on the Coriolis coupling force.

The absolute velocity of a point P with a mass m in the fixed frame R can be expressed as a function of the velocity and the displacement in the rotating frame R':

$$\{\dot{u}(P)\} = \{\dot{u}'(P)\} + \{\Omega\} \wedge \{OP'\} + \{\Omega\} \wedge \{u'(P)\} \tag{5}$$

A second derivative leads to the equilibrium equation in the time domain:

$$m\{\ddot{u}'(P)\} + 2m\{\Omega\} \wedge \{\dot{u}'(P)\} + m\{\Omega\} \wedge \{\Omega\} \wedge \{u'(P)\} + K(u'(P))\{u'(P)\} = \{F\}_c \tag{6}$$

After linearization around the steady state, this equation shows respectively the inertial mass, the Coriolis forces, the centrifugal stiffness and the structural stiffness (which includes the geometrical stiffness):

$$\mathbf{M}\ddot{\mathbf{U}}' + (\mathbf{C} + \mathbf{G}_c(\Omega))\dot{\mathbf{U}}' + (\mathbf{K} + \mathbf{K}_c(\Omega) + \mathbf{K}_\sigma(\Omega))\mathbf{U}' = 0 \tag{7}$$

The centrifugal forces which apply to the initial configuration are in the second term. For a concentrated mass with degrees of freedom in translation and rotation around the Oz axis, these matrices have the following expressions:

- Coriolis pseudo-damping:

$$\begin{Bmatrix} F_x \\ F_y \\ F_z \end{Bmatrix} = \mathbf{G}_c \cdot \begin{Bmatrix} \dot{u}'_x \\ \dot{u}'_y \\ \dot{u}'_z \end{Bmatrix} = \begin{bmatrix} 0 & -2m\Omega & 0 \\ 2m\Omega & 0 & 0 \\ 0 & 0 & 0 \end{bmatrix} \cdot \begin{Bmatrix} \dot{u}'_x \\ \dot{u}'_y \\ \dot{u}'_z \end{Bmatrix} \tag{8}$$

- Centrifugal (negative) stiffness:

$$\begin{Bmatrix} F_x \\ F_y \\ F_z \end{Bmatrix} = \mathbf{K}_c \cdot \begin{Bmatrix} u'_x \\ u'_y \\ u'_z \end{Bmatrix} = \begin{bmatrix} -m\Omega^2 & 0 & 0 \\ 0 & -m\Omega^2 & 0 \\ 0 & 0 & 0 \end{bmatrix} \begin{Bmatrix} u'_x \\ u'_y \\ u'_z \end{Bmatrix} \tag{9}$$

The centrifugal forces can be computed by multiplying the previous matrix with the opposite of the position vector:

$$\mathbf{F}_c = \begin{Bmatrix} m\Omega^2 x_p \\ m\Omega^2 y_p \\ 0 \end{Bmatrix} \tag{10}$$

The aspect of the Coriolis matrix is similar to the gyroscopic matrix and separates real eigenmodes in complex forward and backward modes. A first difference between these two pseudo-damping matrices is the fact the Coriolis matrix concerns—from a physical point of view—translation degrees of freedom and not rotations. Note gyroscopic matrix of beam elements can also include translational degrees of freedom but only because of the element shape functions which link local curvature to node displacement and rotation. A more important difference is the opposite sign, which means the eigenfrequencies of the forward modes decrease with the rotation speed, while those of the backward modes increase. Also, note the negative sign and the proportionality to Ω^2 of the centrifugal stiffness. This implies the apparent stiffness of the rotating system may be cancelled for some values of rotating speed. These particular rotating speeds will be named critical speeds. At these rotating speeds, a natural frequency of the system may become null because of the change of its sign: forward mode may become backward mode above the critical speed.

3.2. 2D Fourier model

Rotating systems are often characterized by their complexity and the necessity of adopting simplifying techniques such as modal reduction or specific finite elements such as beam elements. 2D Fourier finite elements can also be very useful if the structure is—or is assumed to be—axisymmetrical but has flexibility not represented by beam kinematics. 2D Fourier models also show the capability to strongly reduce the problems relative to the modal density of real structures by selecting Fourier harmonics n_θ appropriate to the analysis.

The displacement field is assumed to develop on the Fourier harmonic n_θ. Usually, this field is split into symmetrical and asymmetrical harmonics:

$$u_r(r,z,\theta) = u_r^s(r,z)\cos n_\theta\theta + u_r^a(r,z)\sin n_\theta\theta \tag{11a}$$

$$u_z(r,z,\theta) = u_z^s(r,z)\cos n_\theta\theta + u_z^a(r,z)\sin n_\theta\theta \tag{11b}$$

$$u_\theta(r,z,\theta) = u_\theta^s(r,z)\sin n_\theta\theta + u_\theta^a(r,z)\cos n_\theta\theta \tag{11c}$$

For dynamic calculations, the displacement field varying in function of time can be chosen. The solution adopted here is to choose modulated coordinates:

$$u_r(r,z,\theta,t) = u_r^s(r,z)\cos(n_\theta\theta - \omega t) + u_r^a(r,z)\sin(n_\theta\theta - \omega t) \tag{12a}$$

$$u_z(r,z,\theta,t) = u_z^s(r,z)\cos(n_\theta\theta - \omega t) + u_z^a(r,z)\sin(n_\theta\theta - \omega t) \tag{12b}$$

$$u_\theta(r,z,\theta,t) = u_\theta^s(r,z)\sin(n_\theta\theta - \omega t) + u_\theta^a(r,z)\cos(n_\theta\theta - \omega t) \tag{12c}$$

Forward and backward eigenmodes (or waves) are characterized, respectively, by $\omega > 0$ and $\omega < 0$ (n_θ is assumed to be positive).

If the rotating structure is assumed axisymmetrical—which means the mass and stiffness matrices are assumed isotropic, degrees of freedom in the fixed frame noted U can be used for displacement, velocity and acceleration. The time derivatives for velocity and acceleration bring complementary terms due to the convection of the rotating part [15–17]:

$$\frac{\partial \mathbf{U}'}{\partial t}(r,\theta,z,t) = \frac{\partial \mathbf{U}}{\partial t}(r,\theta,z,t) + \Omega\frac{\partial \mathbf{U}}{\partial \theta}(r,\theta,z,t) \tag{13}$$

The equilibrium equation can be written in the time domain:

$$\mathbf{M}\ddot{\mathbf{U}} + 2\Omega\mathbf{M}\frac{\partial \dot{\mathbf{U}}}{\partial \theta} + \Omega^2\mathbf{M}\frac{\partial^2 \mathbf{U}}{\partial^2 \theta} + (\mathbf{C} + \mathbf{G}_c(\Omega))\left(\dot{\mathbf{U}} + \Omega\frac{\partial \mathbf{U}}{\partial \theta}\right) + (\mathbf{K} + \mathbf{K}_c(\Omega) + \mathbf{K}_\sigma(\Omega))\mathbf{U} = 0 \tag{14}$$

Eqs. (7) and (14) can be written in the frequency domain in order to calculate the natural pulsation of the rotor directly in the inertial frame:

$$\left(-\omega_{\text{rotating}}^2\mathbf{M} + \omega_{\text{rotating}}(\mathrm{i}\mathbf{C} + \mathrm{i}\mathbf{G}_c(\Omega)) + (\mathbf{K} + \mathbf{K}_c(\Omega) + \mathbf{K}_\sigma(\Omega))\right)\mathbf{U}' = 0 \tag{15}$$

$$\left[-(\omega_{\text{fixed}} - n_\theta\Omega)^2\mathbf{M} + (\omega_{\text{fixed}} - n_\theta\Omega)\mathrm{i}\mathbf{G}_c(\Omega) + (\omega_{\text{fixed}} - n_\theta\Omega)\mathrm{i}\mathbf{C} + (\mathbf{K} + \mathbf{K}_c(\Omega) + \mathbf{K}_\sigma(\Omega)\right]\mathbf{U} = 0 \tag{16}$$

The complex eigenfrequencies and eigenmodes corresponding to Eqs. (15) and (16) are calculated in three steps: the real eigenmodes of Eq. (16) without damping terms are determined, Eq. (16) is reduced on the eigenmodes base and the complex eigenmodes are finally calculated.

The comparison of the equilibrium equations in the rotating frame (Eq. (15)) and the fixed frame (Eq. (16)) clearly shows the relationship between the natural pulsations in the rotating and fixed frames:

$$\omega_{\text{rotating}} = \omega_{\text{fixed}} - n_\theta \Omega \tag{17}$$

Since the change between rotating and fixed frames is included directly in Eq. (16), the Fourier formulation presented in this paper allows studying systems with strong coupling between rotor and stator which is of major importance for the global analysis of complex rotating machines.

4. Simple examples for the interpretation of the calculated natural frequencies

Several simple examples of rotating structure represented by full 3D model are analysed in this part. The meaning of the natural frequency computed in the rotating frame is discussed in detail since the same structure analysed in rotating and inertial frames exhibit different natural frequencies.

4.1. Rotating ring

Let us consider a ring with a radius R and a square section of thickness h (Fig. 5). The motion of the ring is limited in the plane Oxy perpendicular to the rotation axis Oz. Its first natural non-null frequency corresponds to a Fourier mode $n_\theta = 2$ and is equal to

$$f_n = \alpha_n \sqrt{\frac{Eh^2}{12(1-\nu^2)\rho R^3}} \quad \text{with } \alpha_2 = 1.34 \tag{18}$$

The natural frequencies of the first two complex modes in the rotating frame have been computed for a rotating speed varying up to three times its first natural frequency. The evolution of the natural frequencies in the rotating frame has been computed taking into account different matrices (Fig. 6). The rotating velocity and natural frequencies have been divided by the first natural frequency at rest in order to obtain dimensionless diagrams.

Fig. 6a shows the evolution of natural frequencies in the rotating frame when only the elastic and geometrical stiffnesses are considered. The centrifugal forces have an important stiffening effect on the first deformation mode of the ring. They also strangely increase the stiffness of the rigid-body eigenmode in

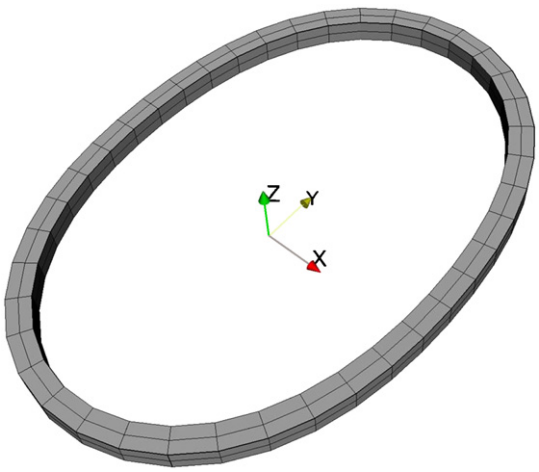

Fig. 5. First in-plane eigenmode of the ring ($n_\theta = 2$).

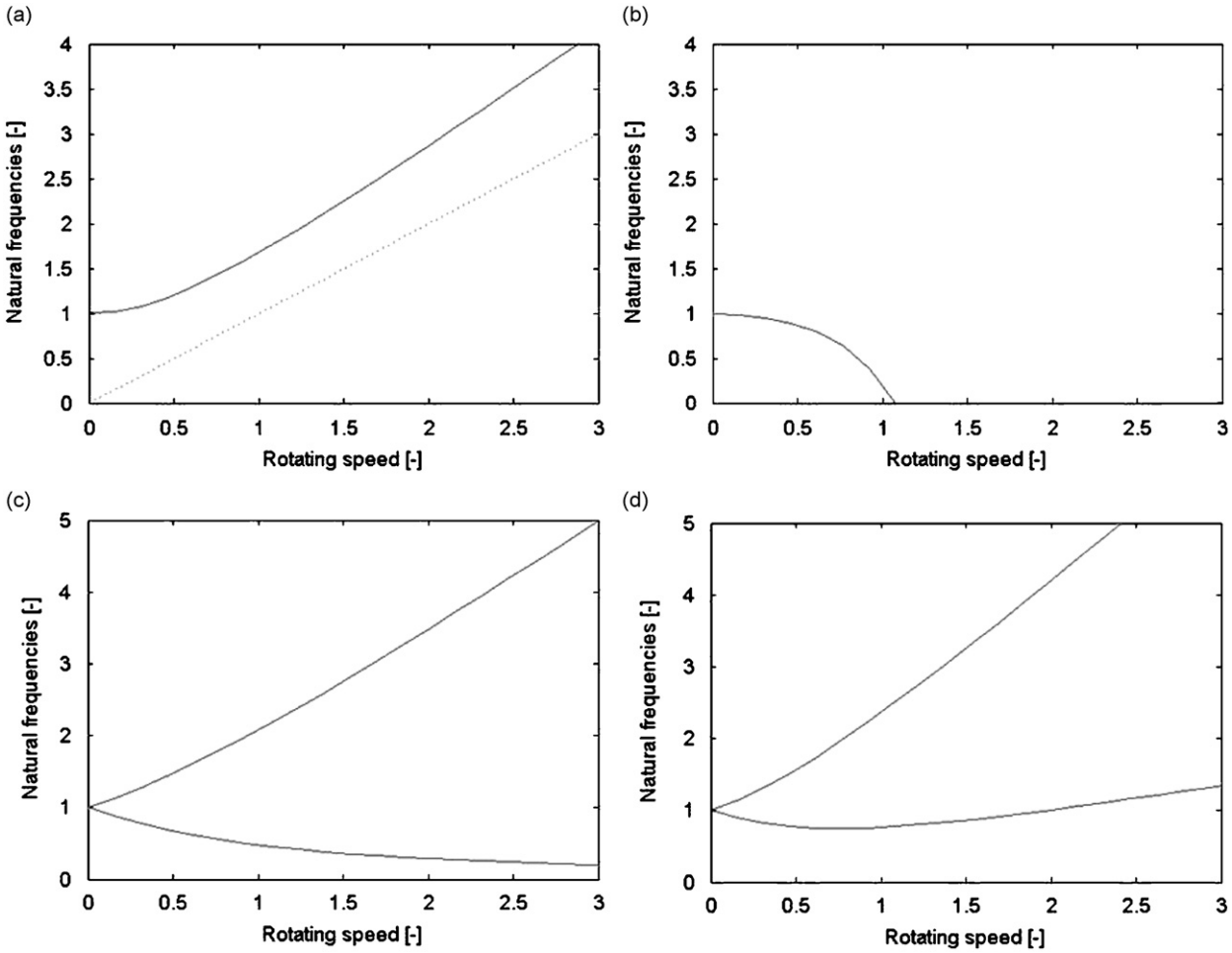

Fig. 6. Evolution of the ring natural frequencies taking into account the different matrices: (a) Geometrical stiffness only. (b) Centrifugal stiffness only. (c) Coriolis coupling only. (d) Geometrical, centrifugal and Coriolis matrices (physically realistic case).

rotation which has not been constrained in the computation: the frequency of this mode is exactly equal to the rotating speed (broken line).

When the elastic and centrifugal stiffnesses are considered (Fig. 6b), the apparent stiffness of the ring is cancelled when the rotation speed becomes equal to the natural frequency of the rotating structure. This can be easily explained when one remembers the form of the centrifugal stiffness. This cancellation of apparent stiffness corresponds to the equality $(K-\Omega^2 M)\Phi = 0$ which is the definition of the undamped eigenmodes. Although the calculation of the critical speed and the associated mode is similar to an elastic buckling analysis, the physical meaning of the critical mode is very different from a buckling eigenmode: above the critical speed, the real system (Fig. 6d) recovers a non-null stiffness. The critical eigenmodes have the same physical nature as the dynamic eigenmodes: the cancellation of the apparent stiffness in the rotating frame corresponds to the resonance in the fixed frame.

The Coriolis coupling separates the real eigenmodes into two complex eigenmodes (Fig. 6c). Note the backward mode has the highest frequency in the rotating frame.

When all the effects are taken into account (geometrical stiffness, centrifugal stiffness and Coriolis coupling), apparent stiffness no longer cancels above the critical speed but only for the critical rotating speed (Fig. 6d): in this case the centrifugal stiffening compensates the negative centrifugal stiffness. It is obvious that only this last calculation has a physical sense and must be carried out.

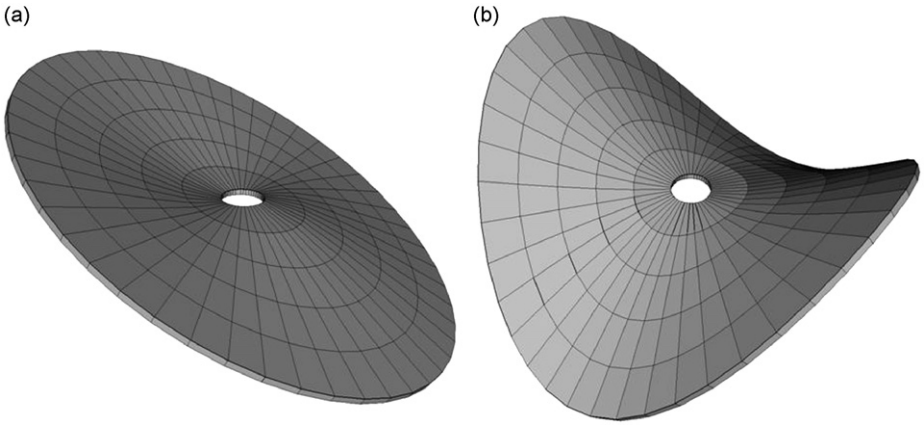

Fig. 7. First out-of-plane eigenmodes of the disc: (a) Mode 1 ($n_\theta = 1$). (b) Mode 2 ($n_\theta = 2$).

4.2. Rotating disc

Let us now study a disc with a radius R and a thickness h. The two first natural eigenmodes at rest have frequencies according to Eq. (18) equal to

- $\alpha_1 = 1.81$ for the first eigenmode which is a Fourier mode $n_\theta = 1$ (Fig. 7a).
- $\alpha_2 = 2.87$ for the second eigenmode which is a Fourier mode $n_\theta = 2$ (Fig. 7b).

The evolution of natural frequencies in the rotating frame has been computed up to a rotating velocity equal to 5 times the first natural frequency at rest. The rotating velocity and natural frequencies have been divided by the first natural frequency at rest. In the rotating frame, the diagram shows few Coriolis effects (Fig. 8) although the computed complex modes can be seen as forward and backward flexural waves. This very low influence of the Coriolis coupling greatly shows the difference between Coriolis and gyroscopic coupling since a disc is very influenced by the gyroscopic coupling: in the inertial frame, when the disc attempts to tilt around one horizontal axis, the gyroscopic forces tend to tilt it around the perpendicular axis which is not the case in the rotating frame. This apparent contradiction can be explained when the natural frequencies calculated in the rotating frame are modified to frequencies in the inertial frame (where the observer is placed). This modification consists in increasing the natural frequency of the forward mode by $n_\theta\Omega$ and decreasing those of the backward mode by $n_\theta\Omega$ where n_θ is the number of spatial periods along the disc perimeter (number of the Fourier modes). This modification induces a separation of the forward and backward modes (Fig. 9). In the inertial frame, the forward modes have the highest frequency, exactly as for the gyroscopic coupling in the beam element. For $n_\theta = 2$ (and for all the cases $n_\theta > 1$), the evolution of the natural frequencies in the inertial frame (Fig. 9b) shows a singularity: for a critical speed close to the natural frequency at rest, the disc shows no apparent stiffness and deforms under static force in the inertial frame (which is a backward rotating force in the rotating frame and can excite the corresponding eigenmodes). This phenomenon, well known for high-speed discs [15–17], can be studied in this way using finite element modelling (FEM) models for realistic geometry and not only with analytical models.

4.3. Rotating disc on a flexible shaft

The natural frequencies of the rotating disc on a flexible shaft supported at each extremity already studied previously with beam elements have been calculated between 0 and 2000 rad/s with 3D finite elements. The first eigenmode (Fig. 10a) has a natural frequency at rest equal to 628 rad/s and corresponds to a global bending mode already caught by the beam model. The second eigenmode is specific to the 3D finite element

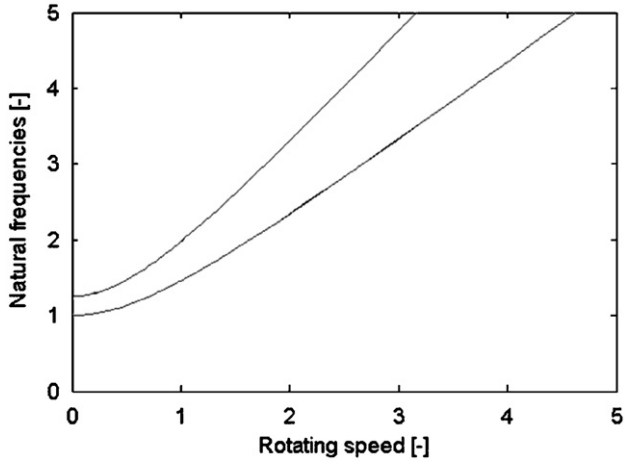

Fig. 8. Evolution of the natural frequencies in the rotating frame ($n_\theta = 1$ and $n_\theta = 2$).

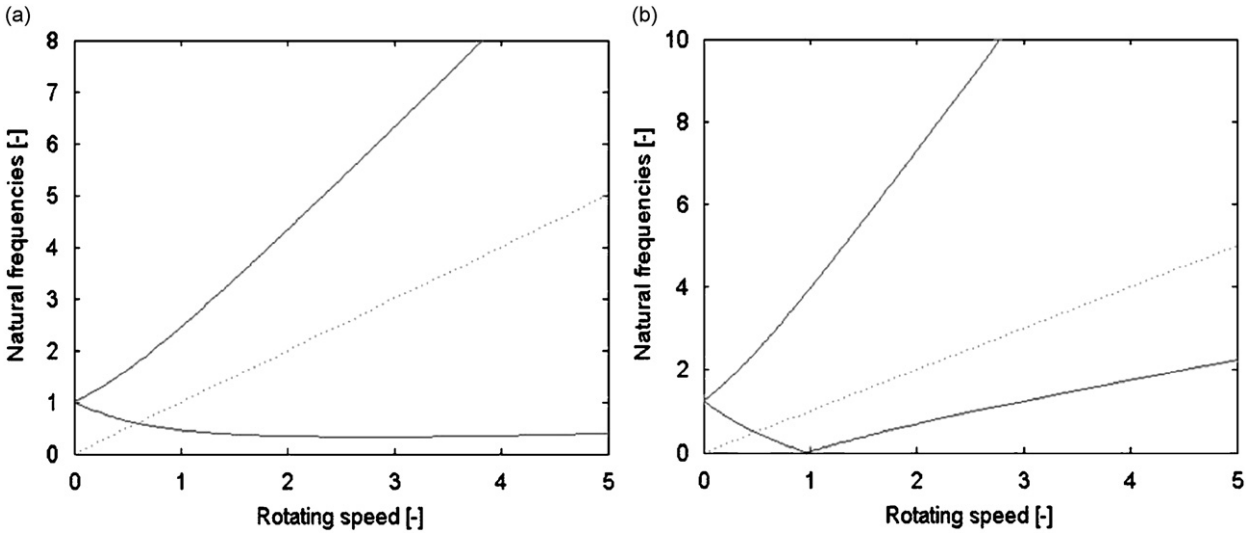

Fig. 9. Evolution of the natural frequencies of the disc in the inertial frame: (a) First eigenmode ($n_\theta = 1$). (b) Second eigenmode ($n_\theta = 2$). Natural frequencies in full line. Synchronous whirl in dashed line.

model since it requires a representation of the disc flexibility (Fig. 10b). Its natural frequency is equal to 974 rad/s.

Let us consider the first global bending eigenmode. In the first part of the diagram, the natural frequencies of the backward and forward modes, respectively, increase and decrease. The direct mode becomes critical at about 700 rad/s, which is slightly higher than the natural frequency at rest (Fig. 11). This difference between the critical speed and the natural frequency can be explained by the gyroscopic coupling in the inertial frame and by the geometrical stiffness (or centrifugal stiffening) in the rotating frame. Above the critical speed, the forward mode becomes a backward mode in the calculation frame (rotating) which means that in the inertial frame the rotating speed is higher than the frequency of the direct mode (Fig. 11b). This example clearly shows that the cancellation of the apparent static stiffness in the rotating frame is nothing other than the resonance in the inertial frame: in both cases, the critical speed corresponds to a null apparent stiffness (static or dynamic) only at the critical speed.

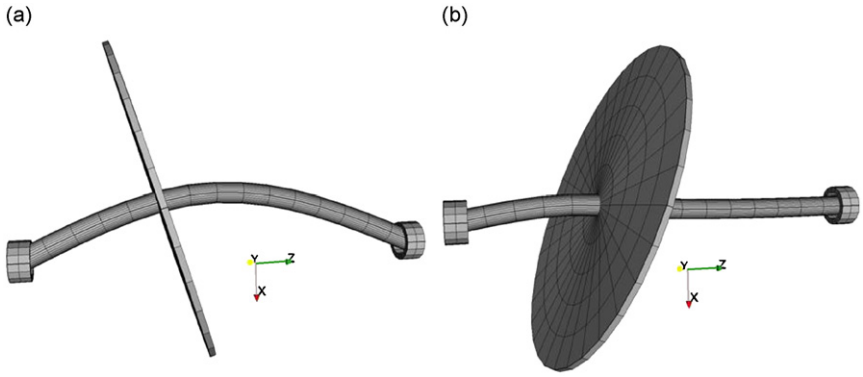

Fig. 10. Eigenmodes of a 3D model of a disc on a flexible shaft: (a) Global bending mode ($\omega_{\text{bending}} = 628$ rad/s). (b) Second eigenmode with disc flexibility ($\omega_{\text{disc}} = 974$ rad/s).

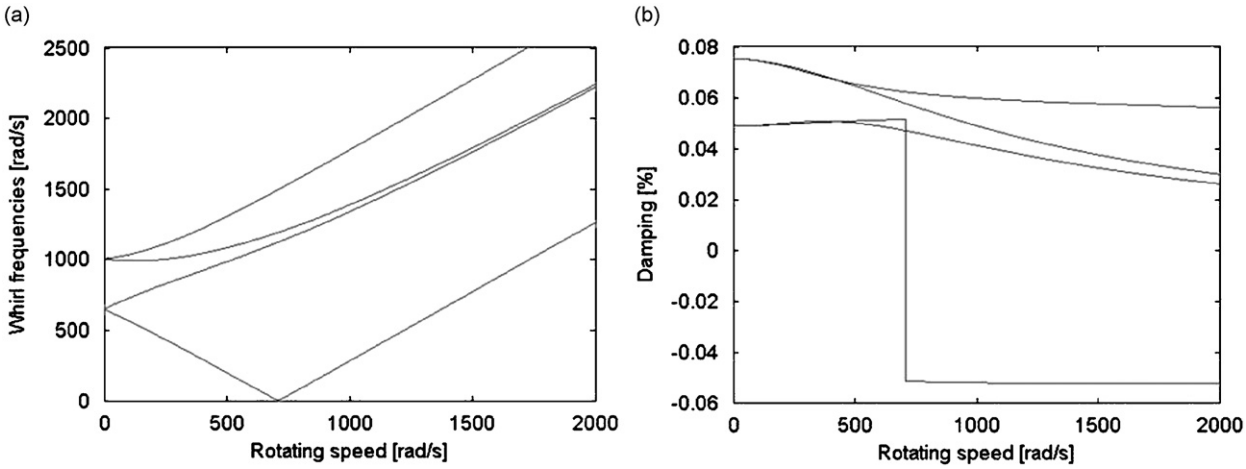

Fig. 11. Evolution of complex frequencies of the rotating disc on a flexible shaft in the rotating frame (3D model): (a) Whirl frequencies. (b) Reduced damping values.

4.4. Conclusions for the analysis in the rotating frame

The previous examples clearly show that a rotating structure represented by full 3D and/or 3D shell elements in the rotating frame can be studied if the Coriolis coupling, the centrifugal stiffness and the geometrical stiffness are taken into account. The natural frequencies and the critical speeds can be determined and the analyses exactly give the same information as the beam model with gyroscopic coupling. The critical speed can also be determined using the same procedure as those for elastic buckling analysis [6,7,11]. The different natures of a same physical phenomenon which is dynamic in the inertial frame and static in the rotating frame can be surprising but one may think about the unbalance loads which are, respectively, rotating (and thus dynamic) and static. Dynamic stability can also be analysed looking at the damping values which can be useful, for example, in the case of interaction between discs and blades [18].

5. Prediction of the unbalance response

The response to unbalance load is often required to check the capacity of a rotating machine to withstand mass and geometrical defects and/or to help in reducing problematic vibration levels.

5.1. Methodology

In the inertial frame, prediction of the unbalance response is harmonic since the unbalance load is a direct rotating force. Such an analysis becomes "static" for the rotor represented in the rotating frame. The apparent contradiction disappears when one compares the spin softening to be taken into account in the rotating frame and the rotor mass impedance necessary for a harmonic calculation in the inertial frame. The "static" nature of the rotor response clearly shows that the response of the rotating shaft is independent of the rotor damping but depends on the fixed damping. This implies that at resonance the response of the shaft is at 90° to the unbalance load (and at 180° for a supercritical speed). Harmonic analysis for the prediction of the vibration under unbalance loads can also be performed with a decomposition of the response of each component on the harmonic frequencies of the rotating speed (including the static response of the rotor). Special attention must be given in the connection between the rotating and the fixed components of the model since the static mode of the rotating part of the machine is linked to the Ω forward mode of the static part for the isotropic system. For a non-isotropic system, the equivalence between inertial and rotating frames is more difficult [8].

Let us consider the former system when the fixed damping is taken into account in order to limit the displacement amplitude at critical speed. Harmonic equation (Eq. (4)) used in the inertial frame in which $F(t)$ is a forward unbalance load corresponds to the following equation which is static in the rotating frame (Eq. (19a) where the centrifugal forces F_c are static) and harmonic in the fixed frame (Eq. (19b)):

$$(\mathbf{K}_c(\Omega^2) + \mathbf{K}_\sigma(\Omega^2) + \mathbf{K}_{\text{rotor}})\mathbf{U}' = \mathbf{F}_c + \mathbf{F}^{\text{static}}_{\text{stator}\Rightarrow\text{rotor}} \tag{19a}$$

$$(-\Omega^2\mathbf{M}_{\text{stator}} + \mathrm{i}\Omega\mathbf{C}_{\text{stator}} + \mathbf{K}_{\text{stator}})\mathbf{U} = \mathbf{F}^{\text{harmonic_direct_}\Omega}_{\text{rotor}\Rightarrow\text{stator}} \tag{19b}$$

For connecting the two frames and avoiding rotor rigid motion, the appropriate conditions are imposed between rotor and stator components using master and slave coordinates. Practically fictitious points are created and linked to the average motion of rings situated on the rotor or stator interfaces (bearings, electric motor, etc.). Since only average stiffness and damping are usually known for bearing, these conditions concern only the transversal mode $n_\theta = 1$ (transverse rotation and translation) and the longitudinal mode $n_\theta = 0$ (axial and torsion motions). In a Cartesian frame, these conditions are applied to the average displacement and rotation. The last step is to express the rotor master coordinates known in the rotating frame (static motion) and in the inertial frame (harmonic motion using complex coordinates) and to link rotor and stator master coordinates in the inertial frame (where stiffness, damping and mass of supports are known Eq. (19b)). These constraints are imposed using Lagrange multipliers which give directly the interaction forces between rotor and stator.

5.2. Application to the disc on flexible shaft

The 3D model of the disc on a flexible shaft has been completed by adding the stator (Fig. 12a). The rotor is represented in the rotating frame and bearings in the inertial frame. At each extremity, the rigid motions are constrained (equivalent to beam elements being simply supported). Isotropic transverse stiffness and damping defined in the fixed frame is fixed at one third of the shaft. The unbalance responses (for the 2° initial tilt on disc) are plotted in Fig. 12b with, on one side, classical beam model in the fixed frame R (full line) and, in the other side, 3D model in both rotating frame R' and fixed frame R (dashed line) frames. Curves show a maximum at the critical speed corresponding to the forward mode (Figs. 2 and 11) and response amplitude is limited by the fixed damping. Because of the disc flexibility, response amplitudes with the 3D and beam models become different (Fig. 12b). The main difference between beam and 3D modelling is the disc flexibility not represented by beam kinematics. Fig. 10b shows the mode dominated by the disc flexibility (axial mode at $n_\theta = 1$ similar to Fig. 7a).

5.2.1. Effect of an initial angular tilt

In order to investigate the effect of disc flexibility, let us analyse a disc with an initial angular tilt $\varphi = 2°$ (or misalignment) with a model in the rotating frame. The disc is similar to the disc on the shaft but is fixed to the rotating frame. Its first natural frequency at rest is noted ω_{disc}. The dimensionless response (axial displacement

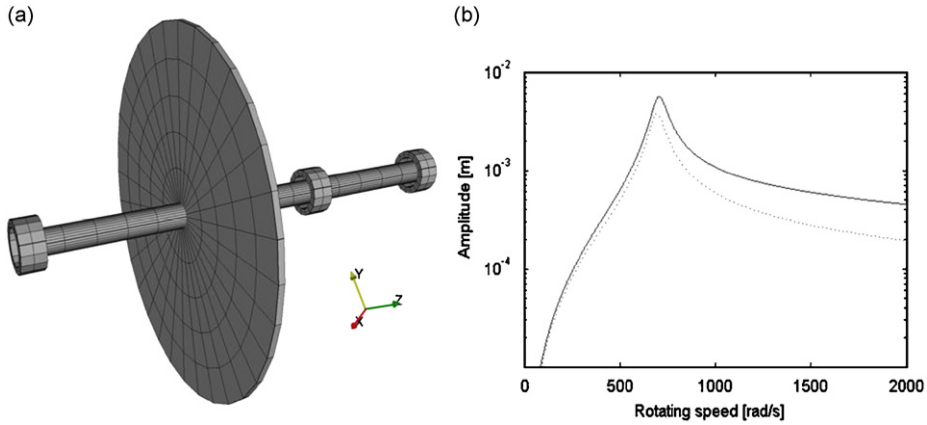

Fig. 12. Unbalance response of a disc on flexible shaft with isotropic bearings: (a) 3D rotor and stator model. (b) Unbalance response. Beam model in full line, 3D model in dashed line.

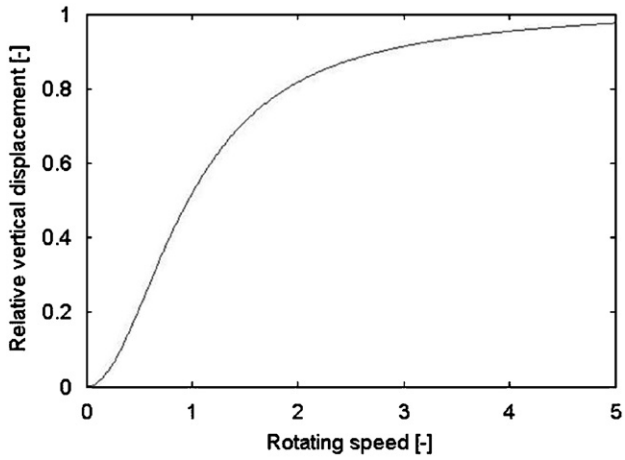

Fig. 13. Analysing of a disc with an angular misalignment (3D model).

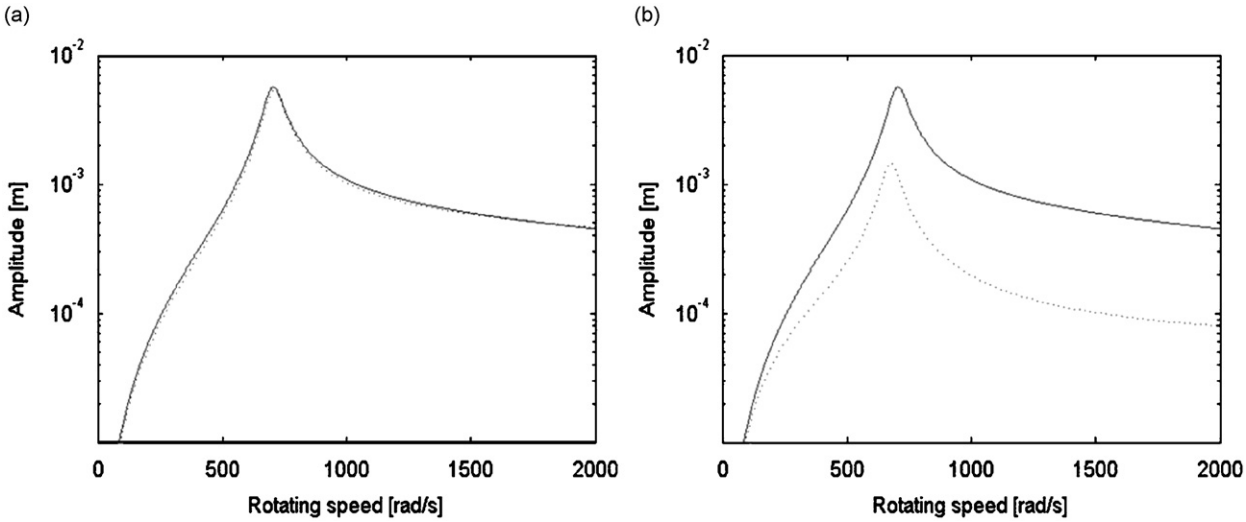

Fig. 14. Unbalance response of the 3D model for different Young modulus of the disc: (a) $E_{\text{disc}} = 100 \times E_{\text{initial}}$. (b) $E_{\text{disc}} = 1/10 \times E_{\text{initial}}$. Beam model in full line, 3D model in dashed line.

divided by the initial vertical defect plotted versus Ω/ω_{disc}) of a peripheral point under an angular tilt has been plotted in Fig. 13: the angular initial tilt is progressively cancelled when the disc rotating speed increases. By analysing different responses under different assumptions (different dimensions and values for φ, types of fault distribution, etc.), it clearly appears the curves always have the same shape and the initial vertical defect tends to vanish when Ω reaches the natural frequency ω_{disc}.

5.2.2. Influence of the disc flexibility on the global shaft bending response

Consider now the example presented in Section 5.2.

In a first step, the disc's Young modulus E has been increased artificially by a factor of 100 compared with Section 5.2. This change has a very low influence on the shaft critical speed $\Omega_{critical}$ but the first natural frequency of the disc ω_{disc} becomes much higher than the first critical speed $\Omega_{critical}$. This means the disc is rigid compared with the shaft and the disc angular misalignment does not vanish for $\Omega_{critical}$. The initial moment

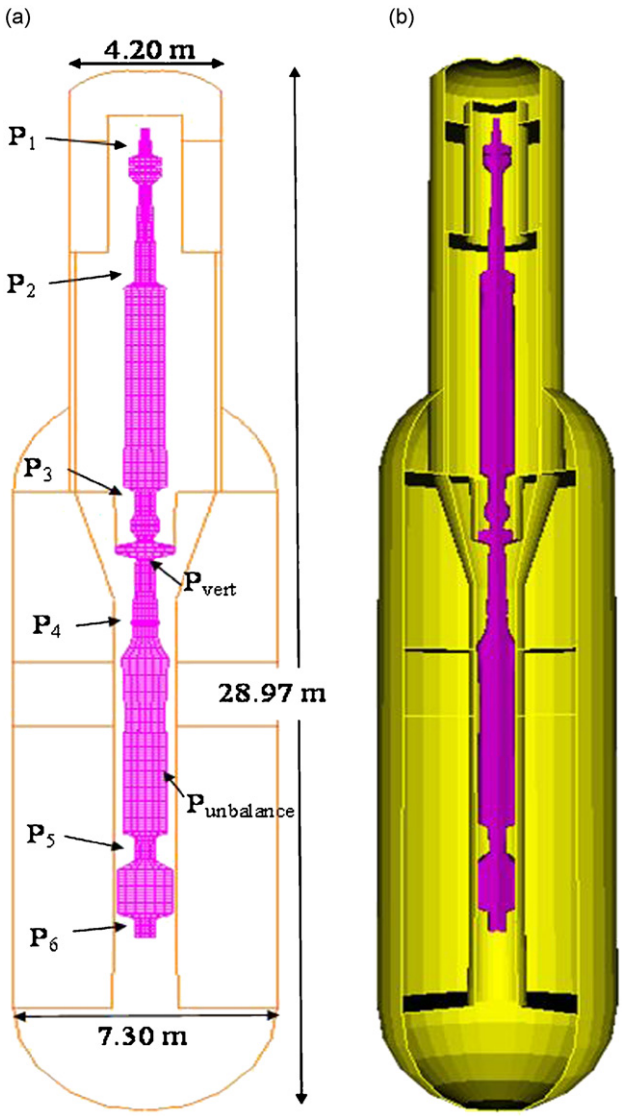

Fig. 15. 2D and 3D representations of the 2D Fourier model of the vertical shaft and the casing of the GTMHR power conversion unit: (a) Main dimensions and 2D mesh. (b) 3D representation.

induced by the disc initial tilt remains as proportional to Ω^2 as for the beam model. Unbalance response is approximately the same for a 3D model and a beam finite element model (Fig. 14a).

In a second step, the disc's Young modulus E has been decreased by a factor of 10. The disc natural frequency ω_{disc} becomes lower than Ω_{critical}. The disc is flexible compared with the shaft and the 2° initial tilt strongly decreases due to the disc flexibility (Fig. 14b). This property is taken into account with the 3D finite element model in the rotating frame. In the 3D model, the moment induced by a disc initial tilt and thus the vibration amplitudes are much lower than for a beam model (couple proportional to Ω^2).

6. Application to the GTMHR vertical shaft

The previous examples concern only simplified rotating structures. In order to show the capability of the modelling tools to be applied to the analysis of complex industrial structures, a numerical model of the GT-MHR vertical turbine and turboalternator unit situated in the power conversion vessel [1,2] has been developed under the 2D Fourier assumptions with $n_\theta = 1$. Stability and forced response analysis very similar to Ref. [19] have been performed at a reasonable cost (few minutes on a 2 GHz PC) with a refined model taking into account flexibilities not represented by a beam model. Since the ambition of the present study is only to show the capability of the modelling approach for complex system, the model does not take into account all the details of the GTMHR power conversion unit.

The main dimensions of the rotating shaft and its casing are given in Fig. 15a. The vertical shaft is supported by vertical thrust magnetic bearings fixed at mid-height (P_{vert}) and by six lateral magnetic bearings

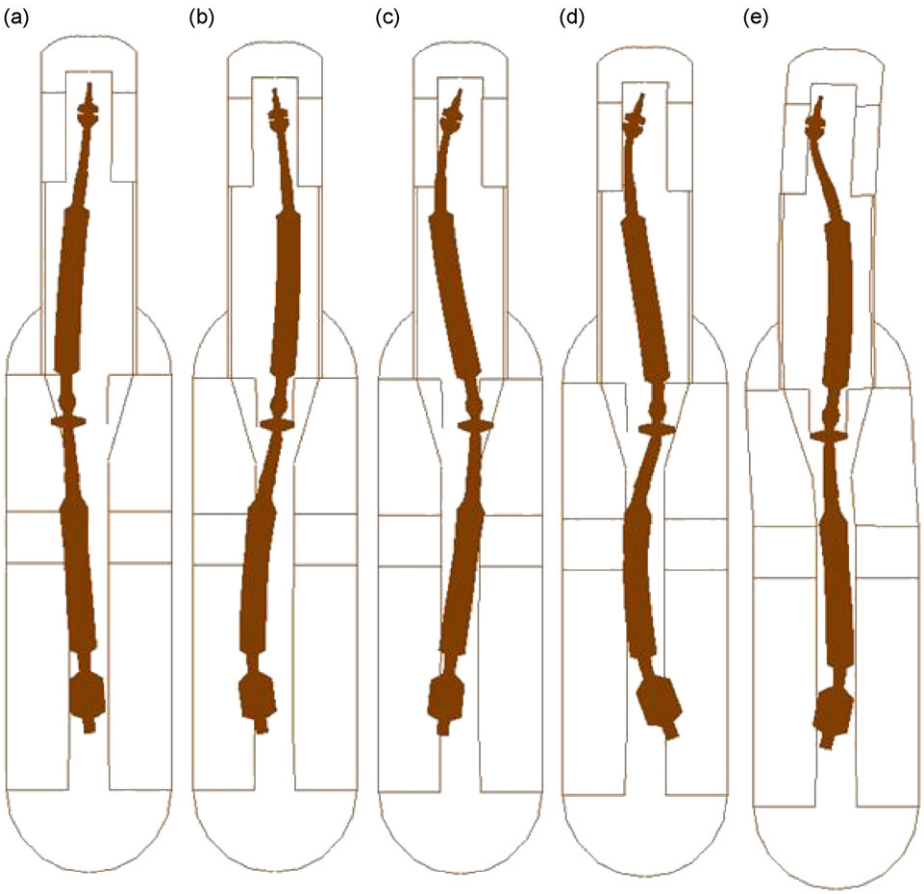

Fig. 16. First eigenmodes at rest of the 2D Fourier model ($n_\theta = 1$): (a) $f_1 = 8.99$ Hz. (b) $f_2 = 13.0$ Hz. (c) $f_3 = 17.8$ Hz. (d) $f_4 = 24.4$ Hz. (e) $f_5 = 33.3$ Hz.

(points P_1–P_6). Fig. 15b shows a 3D representation of the 2D Fourier model. The magnetic bearings are represented in a simplified way by stiffnesses and dampers independent of the rotating speed but a more realistic model in agreement with the real bearing transfer functions can be easily adopted using, for example, equivalent mechanical model with several masses, stiffnesses and dampers. The first eigenmodes at rest are given in Fig. 16. The nominal rotating speed of 3000 rev/min (50 Hz) is above the first flexural eigenmodes of the shaft (Fig. 17) but damping allows going through the critical speed with limited vibrations (Fig. 18). Mass unbalance response is computed for a residual static unbalance of 0.60 kg m situated at point $P_{\text{unbalance}}$ at the compressor stage of the rotating machine. Amplitude of the displacement at the P3 bearing is given in Fig. 18. The forced response of the shaft under an asynchronous loading at the magnetic bearing P3 with constant amplitude between −50 and 50 Hz has also been computed at rest and at nominal speed. The amplitudes of the displacement at P3 bearing are plotted in Fig. 19. Negative values of frequency correspond to backward rotating forces and positive values to forward rotating forces. Note the difference of the responses under backward and forward forces due to gyroscopic coupling. This calculation shows the natural frequencies of the rotating shaft can be clearly evidenced by localized excitations and measurements at the bearing positions. It can be useful to check potential change of eigenmodes due to damage of the rotating machine (for example, evolution of cracks).

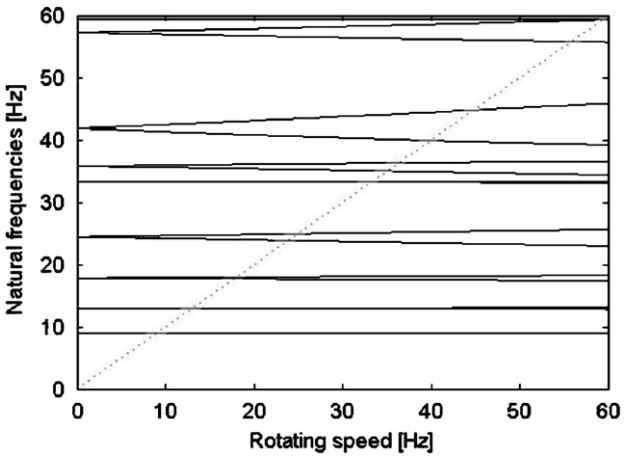

Fig. 17. Evolution of the natural frequencies in the inertial frame. Natural frequencies in full line. Synchronous whirl in dashed line.

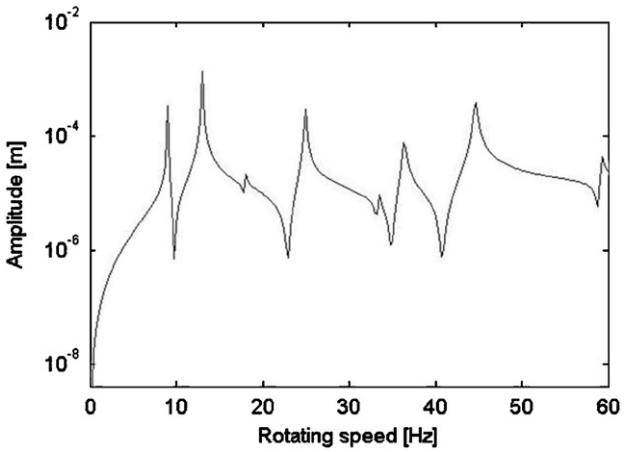

Fig. 18. Unbalance response of the GTMHR shaft. Displacement at the P3 bearing.

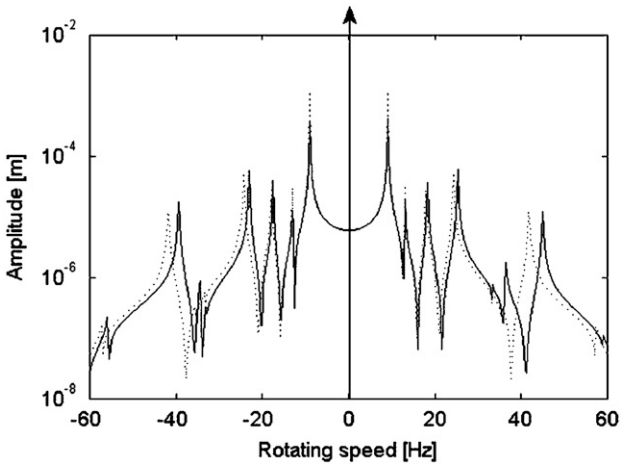

Fig. 19. Harmonic analysis of the shaft. Displacement at the P3 bearing. At rest in broken line. At nominal speed in solid line.

7. Conclusions

This paper has shown the possibility of performing dynamic analyses of complex rotating machines using refined 3D and 2D Fourier finite elements model. The critical rotating speeds and the response to unbalance mass can be determined and the global stability of the machine can be checked. This refined modelling requires supplementary matrices such as Coriolis coupling damping and centrifugal negative stiffness and careful interpretation of the natural frequencies calculated in the rotating frame. This type of modelling coupled with reduction techniques and 2D Fourier assumptions may be very useful to take into account supplementary flexibilities and check stability involving kinematics not represented by beam elements. Refined modelling allows a significant improvement in the prediction of unbalance response of flexible rotating machines which may be overestimated using classical beam models. It will improve the design and the maintenance of large rotating machines like for the GT-MHR nuclear reactors under normal and accidental loading.

References

[1] M.P. LaBar, The gas turbine-modular helium reactor: a promising option for near term deployment, General Atomics, GA-A23952, Website General Atomics: 〈http://www.ga.com/gtmhr/images/ANS.pdf〉, 2002.

[2] AIEA, Gas Turbine Power Conversion Systems for Modular HTGRs, IAEA-TECDOC-1238, 2001.

[3] GT-MHR, Conceptual Design Report, International GT-MHR Project, WBS 1.4.2, Task No. PL-9.4, General Atomics and Minatom, 1988.

[4] CEA, 2006, Les réacteurs nucléaires à caloporteur gaz, Monographie de la Direction de l'énergie nucléaire, e-den, Commissariat à l'Energie Atomique, 2006.

[5] M. Lalanne, G. Ferraris, *Rotordynamics Prediction in Engineering*, second ed., Wiley, New York, 1988.

[6] G. Genta, *Vibration of Structures and Machines*, second ed., Springer, Berlin, 1995.

[7] F. Axisa, *Vibrations sous écoulements, Modélisation des systèmes mécaniques, Tome 4*, Hermès science, 2001.

[8] G. Genta, Whirling of unsymmetrical rotors: a finite element approach based on complex co-ordinates, *Journal of Sound and Vibration* 124 (1) (1988) 27–53 Elsevier, Amsterdam.

[9] A. Nandi, S. Neogy, An efficient scheme for stability analysis of finite element asymmetric models in a rotating frame, *Finite Elements in Analysis and Design* 41 (2005) 1343–1364.

[10] F. Oncescu, A.A. Lakis, G. Ostiguy, Investigation of the stability and steady state response of asymmetric rotors using finite element formulation, *Journal of Sound and Vibration* 245 (2) (2001) 303–328 Elsevier, Amsterdam.

[11] E. Chatelet, F. D'Ambrosio, G. Jacquet-Richardet, Toward global modelling approaches for dynamic analyses of rotating assemblies of turbomachines, *Journal of Sound and Vibration* 282 (2005) 163–178 Elsevier, Amsterdam.

[12] D. Chatelet, D. Lornage, G. Jacquet-Richardet, A three dimensional modeling of the dynamic behavior of composite rotors, *International Journal of Rotating Machinery* 8 (3) (2002) 185–192.

[13] M. Géradin, N. Kill, A new approach to finite element modelling of flexible rotors, *Engineering Computations* 1 (1984).

[14] G. Genta, *Dynamics of Rotating Systems*, first ed., Springer, Berlin, 2005.

[15] A. Raman, C.D. Mote, Experimental studies on the non linear oscillations of imperfect circular disks spinning near critical speed, *International Journal of Nonlinear Mechanics* 36 (2001) 291–305.
[16] J. Tian, S.G. Hutton, On the mechanisms of vibrational instability in a constrained rotating string, *Journal of Sound and Vibration* 225 (1) (1999) 111–126 Elsevier, Amsterdam.
[17] G.L. Xiong, H. Chen, J.M. Yi, Instability mechanism of a rotating disc subjected to various transverse interactive forces, *Journal of Materials Processing Technology* 129 (2002) 534–538.
[18] G. Genta, On the stability of rotating blade arrays, *Journal of Sound and Vibration* 273 (2004) 805–836.
[19] Y. Xu, L. Zhao, S. Yu, Dynamics analysis of very flexible rotor, *Proceedings of the Second International Topical Meeting on High Temperature Reactor Technology*, Beijing, China, 2004.